Dissolution-precipitation-driven upward migration of a salt crust

G. Licsandru,[1,2] C. Noiriel,[1] P. Duru,[2] S. Geoffroy,[3] A. Abou Chakra,[3] and M. Prat[2,*]

[1]*Géosciences Environnement Toulouse (GET), Observatoire Midi Pyrénées, Université de Toulouse, CNRS, IRD, France*

[2]*Institut de Mécanique des Fluides de Toulouse (IMFT), Université de Toulouse, CNRS—Toulouse, France*

[3]*Laboratoire Matériaux et Durabilité des Constructions (LMDC), Université de Toulouse, INSAT, UPS, France*

(Received 14 March 2019; revised manuscript received 16 April 2019; published 5 September 2019)

Salt crusts forming at the surface of a porous medium can dynamically evolve with crust displacements leading to the formations of domes and blisters or simply to the upward migration of the crust. However, the mechanisms explaining the displacements are unclear. It has been conjectured that they could be related to dissolution-precipitation phenomena and/or to mechanical effects associated with the concept of crystallization pressure. We present a simple experiment where the crust upward migration is significant and can be entirely explained from the consideration of dissolution-precipitation phenomena. Equations governing the crust displacement are derived, leading to quite good agreement with the experimental results.

DOI: 10.1103/PhysRevE.100.032802

I. INTRODUCTION

Salt precipitation in porous media is a phenomenon of great importance in various applications such as soil sciences and hydrology [1,2], archelogy and monument preservation [3–5], concrete science [6], and geotechnical engineering [7]. When the precipitation occurs at the surface of a drying porous medium, this process can lead to the formation of a porous salt crust covering the surface [8–12]. The impact of the latter can be quite significant with a reduction of the evaporation rate by more than one order of magnitude [8]. The effect is tentatively explained by considering that the crust acts as a vapor diffusion barrier reducing the vapor transfer rate to the atmosphere [10,13]. However, since this reduction in the evaporation rate can occur when liquid saturation in the medium is quite high and the salt water solution is almost perfectly wetting the crystals [14], it is difficult to explain why the crust would be dry and not wetted by the solution rising into the crust by capillary forces. Interestingly, it has also been shown [15,16] that blistering phenomena could occur. This corresponds to zones where the salt crust is actually not in contact with the porous medium surface anymore with some air trapped between the crust and the porous medium surface. The formation of the air layer, which can be on the order of a few millimeters, i.e., on the order of the capillary length, or much greater under field conditions [15], could locally prevent the solution from rising into the crust by capillarity and might be instrumental in the diffusion barrier scenario. Then, the air layer formation must be explained. This point is very briefly discussed in [15] with the qualitative evocation of the possible role of dissolution-precipitation mechanisms and/or mechanical effects, the latter being suspected in relation with the well-known fact that crystallization in pores can lead to stress generation [4,5,7,17]. Actually, one must realize that the physics of salt crusts is an unexplored area. There has been little work done on going beyond speculative discussions and proposing a model of what happens in a moving salt crust. In this context, the objective of the present paper is to start filling this gap. More specifically, we present an experiment showing unambiguously that a salt crust can migrate upward as a result of dissolution-precipitation phenomena and that this motion can be modeled without consideration of mechanical effects (i.e., stress generation), at least in the conditions of our experiment.

Before going into the details of this experiment, we show in Fig. 1 an illustration of the crust upward migration phenomenon in a drying laboratory experiment. In this experiment, a random packing of glass beads (of diameters in the range 1–50 μm) saturated with a NaCl aqueous solution of salt, mass fraction 0.25, was put in a cylindrical container open on top and exposed to drying at room temperature ($T \sim 22\,^{\circ}$C). As a result of evaporation, a salt crust formed on top of the porous medium. After a while, the phenomenon of interest for the present paper occurred. The crust moved upward and a detachment zone became visible, as illustrated by the gap which can be seen in Fig. 1. In other words, the crust slightly detached from the porous medium. Further analysis of this drying experiment is out of the scope of the present paper. The focus is on the explanation of the phenomenon illustrated in Fig. 1. Actually, the region indicated as the crust in Fig. 1 can be decomposed itself into an upper crust where few glass beads, if any, are present and a lower crust where precipitated salts and glass beads are both present. This will be discussed in detail in a future publication.

The paper is organized as follows. In Sec. II the experimental setup is described. Equations governing the crust displacement are derived in Sec. III. In Sec. IV, the results obtained with the model are compared to the experimental results and a discussion is presented. Conclusions are drawn in Sec. V.

II. EXPERIMENTAL SETUP

As sketched in Fig. 2, a salt crust was "suspended" in a transparent Hele-Shaw cell. The cell was filled with pure

*mprat@imft.fr

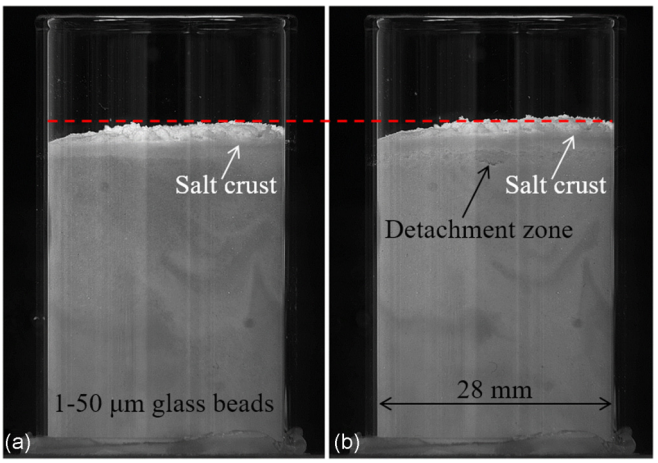

FIG. 1. Illustration of the upward migration of salt crust in a basic drying experiment performed in a cylindrical container filled with glass beads. The elapsed time between the two images (a,b) is 18 days. (b) An elongated gap is visible in the detachment zone (at the end of the black arrow).

liquid water up to a certain height at the bottom of the cell. The liquid water was not in contact with the crust but located at distance $h_b(\sim 9\,\text{mm})$ from the crust bottom surface. The cell was positioned in a transparent enclosure at controlled temperature ($T \sim 22\,^{\circ}\text{C}$) and relative humidity ($H_{r,\text{inf}} \sim 40\%-50\%$), which were both recorded all during the experiment using a Rotronic HygroFlex HTS22X with a Rotronic HygroClip IC05 probe. The mass evolution of this system was measured by placing it on a Mettler-Toledo AX205 precision scale. The solution mass loss was measured at 1-s intervals with data automatically recorded on a computer. A Nikon D800E camera with a resolution of 7360 pixels × 4912 pixels was set to take side view pictures of the cell. Images of the crust and water level in the cell were recorded using as acquisition software Nikon Camera Control Pro 2.26.0 at 1000-s intervals. The pictures were exported thanks to the IMAGEJ© software to analyze the crust motion by tracking the bottom and top crust-gas interfaces.

The suspended crust was obtained during a drying experiment at room temperature. The cell was filled up to a certain height with glass beads (of diameters in the range 1–50 μm) saturated with a NaCl aqueous solution of salt, mass fraction ~0.25. As a result of drying, a crust formed on top of the glass bead packing. After about 4 days, the drying was stopped and the beads were carefully removed from the cell bottom so as to obtain the suspended crust. The crust shown in Fig. 2 actually corresponds to the upper half of the crust so obtained. The lower part where beads are trapped has been removed, so there are little to no beads present in the crust shown in Fig. 2.

Note that the cell is rendered hydrophobic by silanization in order to avoid as much as possible the salt creeping phenomenon, e.g., [18], along the inner wall of the cell. In what follows the mechanical equilibrium of the suspended crust within the cell, especially why the crust sticks to the cell wall, will not be discussed. It is an interesting topic which certainly deserves to be investigated. However, it is our belief that this is not necessary to explain and predict the crust migration within the cell.

As explained in Appendix A, the direct exploitation of measured mass loss and relative humidity $H_{r,\text{inf}}$ led to some inconsistencies between the evaporation rate computed from the measured mass loss and the evaporation rate computed from the position of the crust limiting surfaces within the cell. This led to determine a parasitic mass loss and to introduce a correction on $H_{r,\text{inf}}(t)$ (details are given in Appendix A).

III. RESULTS

The major result is illustrated in Fig. 3. The crust moves upward during the experiment. The migration is quite noticeable, on the order of 1.5 mm, thus comparable here to the capillary length [$l_c = \sqrt{\frac{\gamma}{\rho g}} \approx 2.6$ mm for a NaCl saturated solution, and about twice as much as the initial thickness h_0 of the crust ($h_0 \sim 0.8$ mm, as show in the inset in Fig. 4)]. Also, the shape of the crust does not change appreciably during the displacement (see the movie in the Supplemental Material [19]). As a result, this crust displacement regime is qualified as compact. We can now focus on the mechanisms controlling the displacement and the derivation of equations able to predict the observed displacement.

More details on the crust upward displacement are shown in Fig. 4 together with the results of a model which is presented below. The experimental data shown in Fig. 4 are the arithmetic average of the data extracted from 11 out of

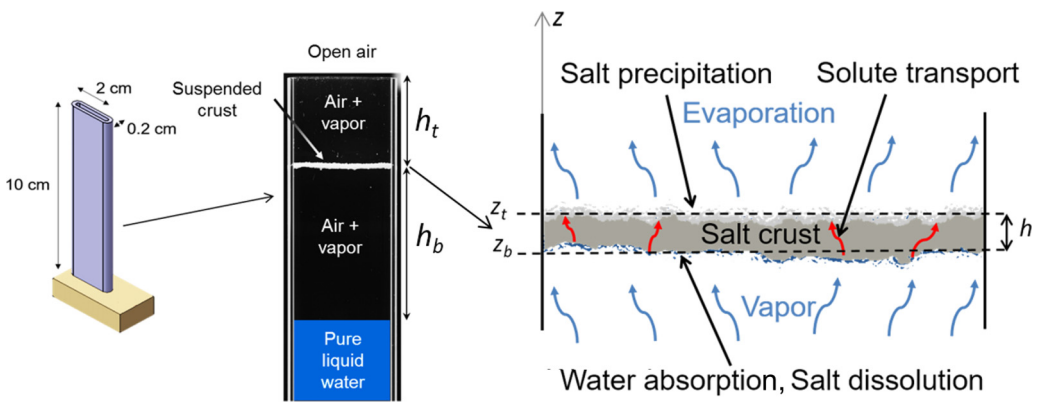

FIG. 2. Schematic of the suspended crust experiment.

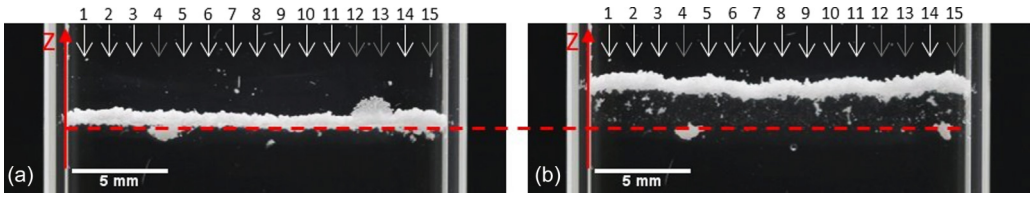

FIG. 3. Comparison between the initial position of the crust in the cell (a) and its final position (b). The red line approximately corresponds to the initial position of the lower surface of the crust. The elapsed time between the two images is about 18 days. The white arrows indicate approximately the position of the vertical pixel lines considered to extract the data shown in Fig. 4.

15 vertical pixel lines evenly distributed over the crust image width at 100-pixel intervals. These lines correspond to the arrows shown in Fig. 3. Lines 4 and 15 were excluded due to the presence of residual beads, visible in Fig. 3, initially in contact with the crust bottom; also lines 12 and 13 were excluded due to a creeping spot, visible in Fig. 4(a), thus rendering them unusable. As indicated in Fig. 4, one can distinguish two main periods. During the first period of about 13 days, the thickness of the crust fluctuates around the value ~0.85 mm. In the second period (day 13 to day 18), there is first a noticeable increase in the crust thickness. Then the crust top surface motion noticeably slows down and the crust thickness stabilizes around 0.95 mm.

IV. MODELING

The mechanisms at play are discussed in what follows from a simple one-dimensional (1D) model considering that the crust is porous [13] and assuming that the crust pores are filled by a NaCl saturated solution (due to the absorption of water vapor resulting from the evaporation of liquid water at the cell bottom). Since the equilibrium vapor pressure of a NaCl saturated solution is $0.75p_{vs0}$ where p_{vs0} is the saturation vapor pressure for pure water, then there is a water vapor transport by diffusion in the gas phase between the liquid water at the bottom and the lower surface of the crust together with evaporation driven by diffusion at the top surface of the crust. Under the classical quasisteady assumption, the corresponding mass fluxes j_b (vapor absorption flux at the crust bottom surface) and j_t (evaporation flux from the crust top) can be expressed as

$$j_b = D_v \frac{M_v}{RT} p_{vs0} \frac{(1 - H_{r,s})}{h_b}, \tag{1}$$

$$j_t = D_v \frac{M_v}{RT} p_{vs0} \frac{(H_{r,s} - H_{r,\mathrm{inf}})}{h_t}, \tag{2}$$

where D_v is the binary diffusion coefficient of the vapor in gas phase, R is the universal gas constant, M_v is the vapor molecular weight, $H_{r,s}$ is the relative humidity at the surface of the NaCl saturated solution ($H_{r,s} = 0.75$), $H_{r,\mathrm{inf}}$ is the relative humidity at the top of the cell. One can refer to Fig. 2 for the definition of the lengths h_b and h_t indicated in Eqs. (1) and (2). These fluxes induce a flow in the pore space of the crust and thus the transport of ions from the crust bottom surface where dissolution must occur, owing to the absorption of pure water to the crust top surface where evaporation and thus precipitation take place (as schematically illustrated in Fig. 2). Within the framework of the classical continuum approach to porous media [20], the convection-diffusion equation governing the ions transport within the crust is

$$\varepsilon\rho \frac{\partial C}{\partial t} + \rho V \frac{\partial C}{\partial z} = \frac{\partial}{\partial z}\left(\rho \varepsilon D_s^* \frac{\partial C}{\partial z}\right) - (1 - C) a_v \rho k_r (C - C_{\mathrm{sat}}), \tag{3}$$

where ρ is the density of the solution, C is the ion mass fraction in the solution, C_{sat} is the equilibrium ion mass fraction in a saturated solution ($C_{\mathrm{sat}} = 0.264$), ε is the crust porosity, V is the filtration velocity, D_s^* is the effective diffusion of the ions, a_v is the pore wall surface area per unit volume, and k_r is the reaction (dissolution or precipitation) coefficient.

Then we express the mass balance on the crust moving top surface for the solution as [21]

$$\rho V = [\rho\varepsilon + \rho_{\mathrm{cr}}(1 - \varepsilon) - \rho_v] \frac{dz_t}{dt} + j_t \quad \text{at } z = z_t, \tag{4}$$

where ρ_{cr} is the crystal density and ρ_v is the vapor concentration.

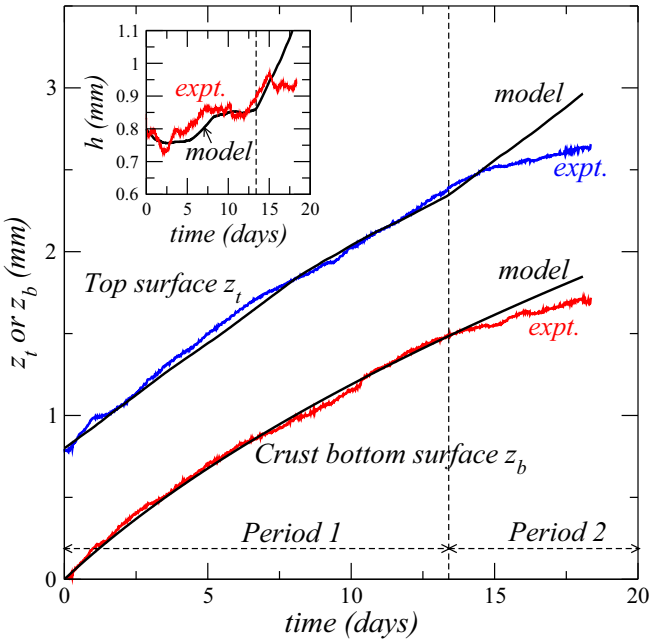

FIG. 4. Crust top and bottom surface positions as a function of time. The inset shows the changes in crust thickness as a function of time. The vertical dashed line corresponds to the end of period 1 (see text).

Similarly, the mass balance for the ions at the crust top surface reads

$$\rho CV - \rho\varepsilon D_s^* \frac{\partial C}{\partial z} = [\rho C\varepsilon + \rho_{\rm cr}(1-\varepsilon)]\frac{dz_t}{dt} \text{ at } z = z_t, \quad (5)$$

Similarly, the mass balance equations on the crust moving bottom surface for the solution and the ions are expressed, respectively, as

$$\rho V = j_b + [\rho\varepsilon + \rho_{\rm cr}(1-\varepsilon) - \rho_v]\frac{dz_b}{dt} \text{ at } z = z_b, \quad (6)$$

$$\rho CV - \rho\varepsilon D_s^* \frac{\partial C}{\partial z} = [\rho C\varepsilon + \rho_{\rm cr}(1-\varepsilon)]\frac{dz_b}{dt} \text{ at } z = z_b. \quad (7)$$

Multiplying Eq. (4) by C and subtracting Eq. (5) leads to (where ρ_v has been neglected since $\rho_v \ll \rho_{\rm cr}$ and $\rho_v \ll \rho$)

$$\frac{dz_t}{dt} = \frac{C_{\rm sat} j_t - \rho\varepsilon D_s^* \frac{\partial C}{\partial z}}{\rho_{\rm cr}(1-\varepsilon)(1-C_{\rm sat})}. \quad (8)$$

Similarly,

$$\frac{dz_b}{dt} = \frac{C_{\rm sat} j_b - \rho\varepsilon D_s^* \frac{\partial C}{\partial z}}{\rho_{\rm cr}(1-\varepsilon)(1-C_{\rm sat})}, \quad (9)$$

where we have assumed $C \sim C_{\rm sat}$ at $z = z_t$ or z_b.

The ion mass fraction gradients in Eqs. (8) and (9) are the gradient at the crust top surface [Eq. (8)] and bottom surface [Eq. (9)], respectively. The displacement rates are also expressed using a macroscopic version [22] of the relationship modeling the precipitation-dissolution reaction within the framework of the diffusion reaction theory [23], namely,

$$\frac{dz_t}{dt} = \frac{\rho}{\rho_{\rm cr}} k_r (C_{\rm top} - C_{\rm sat}), \quad (10)$$

$$\frac{dz_b}{dt} = \frac{\rho}{\rho_{\rm cr}} k_r (C_{\rm sat} - C_{\rm bot}), \quad (11)$$

where $C_{\rm top}$ and $C_{\rm bot}$ are the ion mass fraction at the top and bottom surfaces of the crust, respectively. Then it can be argued that the convective term in Eq. (3) can be neglected from the estimate of the Péclet number Pe characterizing the competition between the convective and diffusive transports of the ions within the crust: ${\rm Pe} = \frac{j_t h}{\rho\varepsilon D_s^*}$ [24]. The evaporation velocity $V_{ev} = \frac{j_t}{\rho}$, as can be computed from Eq. (1), is on the order of 10^{-8} m/s [as indicated by Eq. (4), the filtration velocity induced in the crust is actually higher than the evaporation velocity but of comparable order of magnitude]. With $h \sim 0.7$ mm and, for simplicity, $\varepsilon D_s^* \sim D_s$ where $D_s \approx 1.3 \times 10^{-9} {\rm m}^2/{\rm s}$ is the molecular diffusion of ions in solution, one obtains ${\rm Pe} \sim 0.006$. As expected ${\rm Pe} \ll 1$. Then, it can be argued that the ion distribution within the crust is quasisteady since the characteristic time for diffusion, $t_D \approx \frac{h^2}{D_s} \approx 490$ s, is quite short compared to the characteristic time of the crust displacement (about 2 weeks according to Fig. 4). As a result, Eq. (3) can be simplified as

$$\frac{\partial}{\partial z}\left(\rho\varepsilon D_s^* \frac{\partial C}{\partial z}\right) = (1-C) a_v \rho k_r (C - C_{\rm sat}). \quad (12)$$

Assuming that the porosity of the crust is spatially uniform within the crust and varies little during the displacement (consistently with the fact, as we shall see, that the ion mass fraction is very close to the equilibrium ion mass fraction over most of the crust), Eq. (12) can be solved analytically (details are given in Appendix B).

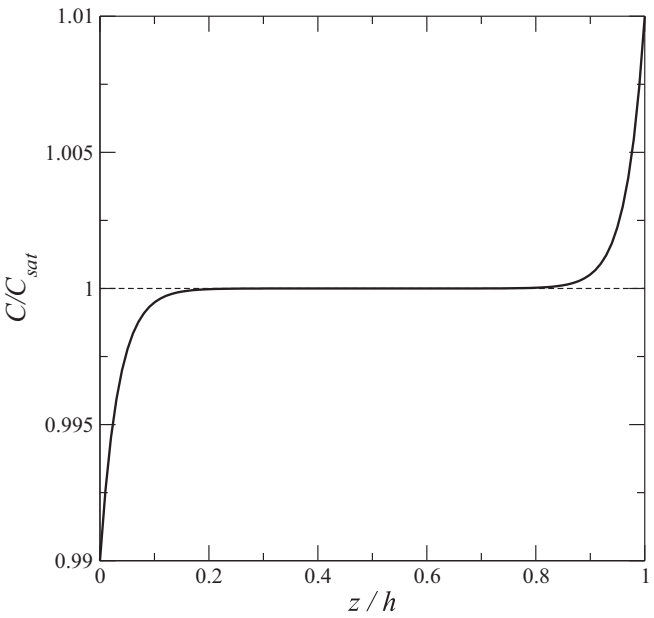

FIG. 5. Typical computed ion mass fraction profile along the crust thickness. The crust bottom and top surfaces correspond to $z = 0$ and $z/h = 1$, respectively.

A typical profile so obtained is shown in Fig. 5. The ion mass fraction is different from the equilibrium ion mass fraction $C_{\rm sat}$ only in the vicinity of the crust top and bottom surfaces. The ion mass fraction is lower than $C_{\rm sat}$ near the crust bottom surface consistently with the occurrence of a dissolution process, whereas C is greater than $C_{\rm sat}$ near the crust top surface consistently with the occurrence of a precipitation process. The fact that C is close to $C_{\rm sat}$ even in the regions where precipitation or dissolution occurs is a consequence of the high value of the reaction coefficient $k_r \approx 2.3 \times 10^{-3}$ m/s [25]. The most important point, however, is the existence of a noticeable ion mass gradient at the crust top and bottom surface. As we shall see, this gradient is sufficiently high for the term $\varepsilon D_s^* \frac{\partial C}{\partial z}$ in Eqs. (8) and (9) to have an impact on the displacement velocity of each surface. In other words, the crust displacement velocity does depend on the ion distribution within the crust. By exploiting the analytical solution to Eq. (12) closed form expressions for the crust surface, displacement velocities can be derived (see Appendix B),

$$\frac{dz_t}{dt} = \frac{C_{\rm sat} j_t}{\rho_{\rm cr}(1-\varepsilon)(1-C_{\rm sat})}\left[\frac{\rm Da}{1+{\rm Da}}\right], \quad (13)$$

$$\frac{dz_b}{dt} = \frac{C_{\rm sat} j_b}{\rho_{\rm cr}(1-\varepsilon)(1-C_{\rm sat})}\left[\frac{\rm Da}{1+{\rm Da}}\right], \quad (14)$$

where ${\rm Da} = \frac{(1-\varepsilon)(1-C_{\rm sat})\lambda k_r}{\varepsilon D_s^*} = \sqrt{\frac{(1-\varepsilon)^2(1-C_{\rm sat})k_r}{\varepsilon D_s^* a_v}}$ is a Damköhler number characterizing the competition between the precipitation-dissolution reaction and the diffusive ion

transport [23]; $\lambda = \sqrt{\frac{\varepsilon D_s^*}{(1-C_{sat})a_v k_r}}$ is a length characterizing the extent of the gradient edge zones illustrated in Fig. 5 (see Appendix B).

V. DISCUSSION

Equations (13) and (14) make clear that the crust displacement velocity depends on the competition between the precipitation-dissolution reaction and the diffusive ion transport. In order to use Eqs. (13) and (14), some properties of the crust (i.e.,ε, a_v, D_s^*) must be specified. However, crusts are thin and fragile porous media for which conventional characterization methods are difficult to use. The result is that these properties are actually not known. From the scanning electron microscopy (SEM) image of the crust surface shown in [13], it is reasonable to assume that the porosity of the crust is low. We have taken $\varepsilon = 0.1$. Then we have checked whether the above model led to good results by fitting the value of the Damkhöler number Da. The value Da = 4.07 leads to the quite good results shown in Fig. 4 [obtained from the numerical solution of Eqs. (13) and (14) using a first order temporal scheme and after correction of the measured relative humidity $H_{r,\text{inf}}$ and consideration of a parasitic leakage as explained in Appendix A), at least during the first period. The crust thickness predicted by the model and shown in the inset of Fig. 4 is simply obtained from the relationship $h = z_t - z_b$. Such a value of Da is obtained, for instance, for the following values of parameters estimated from classical relationships for packing of monodisperse spheres: a mean "grain" radius $r_b = 0.6\,\mu$m corresponding to small pores on the order of 1 μm or less (consistently again with the SEM image of salt crust in [13]); $\varepsilon = 0.05$, $a_v = \frac{3(1-\varepsilon)}{r_b}$ [26]; $D_s^*/D_s = \varepsilon^{0.4}$ [27]. Such a value of the Damköhler number can be also obtained with $r_b \approx 1.5\,\mu$m and $\varepsilon = 0.1$. Although the crust is different from a random packing of spherical particles, we surmise that the corresponding values are consistent with a low porosity compact crust with submicronic to micronic pores.

Also, it is interesting to comment on the value of the Damköhler number Da in our simulations. The crust displacement velocity becomes independent of Da for sufficiently large Da. This corresponds, for instance, to the situation where the precipitation-dissolution reaction would be quite fast compared to the diffusive transport. In this limit, the crust displacement velocity is independent of the reaction parameter k_r. On the contrary, for lower Da the crust velocity displacement depends on the reaction kinetics as in the case of our experiments. The fact that the model leads to less-good results in the second period can be explained as follows.

As depicted in Fig. 6, the first period of about 13 days corresponds to a period in which the evaporation flux j_t from the crust top surface is about the same as the water absorption flux j_b on the crust bottom surface. Since the crust moves upward, i.e., gets closer to the cell top, the evaporation flux is expected to increase whereas the absorption flux is expected to decrease. However, the impact of the distance variation is offset by the increase in the relative humidity $H_{r,\text{inf}}$ at the cell top during the first period (the variation of $H_{r,\text{inf}}$ is depicted in the inset of Fig. 6). This relative humidity increase explains the relatively long period when the two fluxes are comparable.

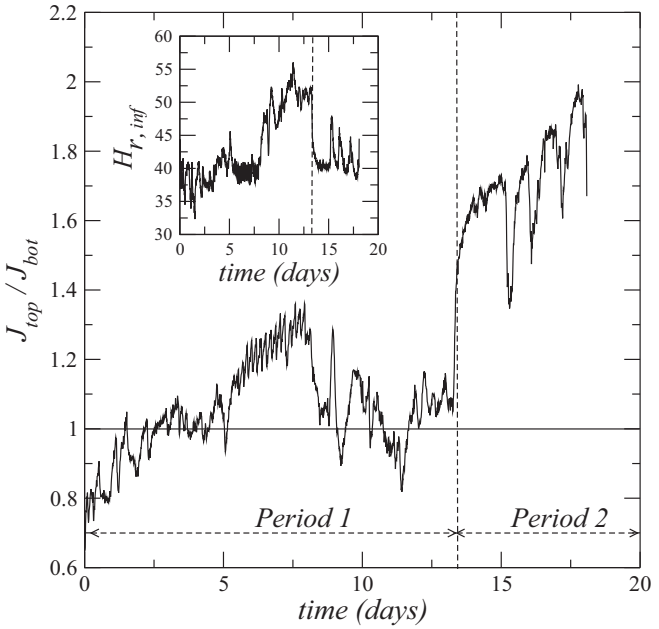

FIG. 6. Ratio between the evaporation rate from the crust top surface and the water absorption rate on the crust bottom surface. The inset shows the variation of the relative humidity at the cell top. As it can be seen the relative humidity is not constant in the experiment due to variations in the room humidity conditions affecting the humidity in the enclosure in which the cell is positioned.

In the second period, the evaporation rate becomes greater than the absorption rate and this introduces a change in the crust migration regime. It is likely that the crust starts drying, which makes the modeling of the second period much more challenging. This is also an indication that various regimes of crust migration must exist. Identifying and studying these regimes is an open interesting question.

Finally, the model can be used not only to predict the crust displacement but also to compute the variation of the liquid level at the bottom of the cell, and thus the variation of the distance $h_b(t)$ between the crust lower surface and the liquid level as well as the total mass loss of the system. This is performed taking into account the parasitic mass loss and the corrected $H_{r,\text{inf}}$ (see Appendix A). As shown in Fig. 7, the variation of the system mass is well reproduced [Fig. 7(b)] whereas the distance between the liquid level and the crust bottom surface is a bit underestimated [Fig. 7(a)] by the model. The trend is, however, quite good, which can be seen as an additional validation of the model.

Then, we have to discuss further the link between the suspended crust experiment and the situations, as illustrated in Fig. 1, motivating the present study, i.e., the phenomena occurring in the crust on top of a porous medium exposed to evaporation.

This link is pictorially illustrated in Fig. 8. Referring to the situation of a salt crust on top of a drying porous medium, it is expected that a vapor pressure gradient forms in the medium as a result of the ion preferential transport towards the top [24] where they feed the crust. Since the lower the ion concentration, the greater is the vapor pressure, this should induce a water vapor flux within the porous medium in the

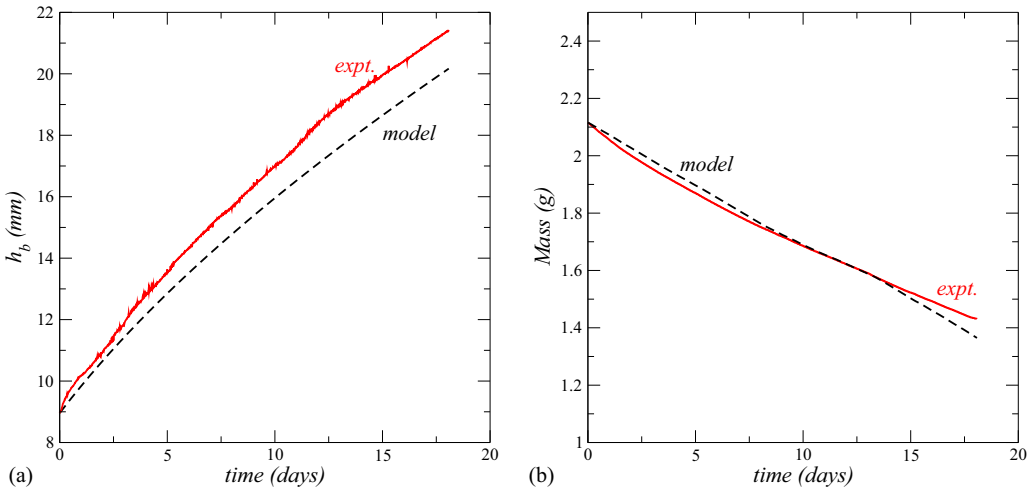

FIG. 7. Comparison between model and experiment: (a) distance $h_b(t)$ between crust bottom surface and liquid level in the cell as a function of time; (b) total mass loss $m(t)$ as a function of time.

direction of the crust, leading to water absorption at the crust bottom. The situation would then be comparable to the situation in our experiment with water vapor absorption coupled with dissolution at the crust bottom and evaporation and precipitation on the top. Confirming this scenario is one interesting topic for future research. A temperature inside the porous medium higher than at the surface can also contribute to the occurrence of the internal vapor flux toward the crust bottom.

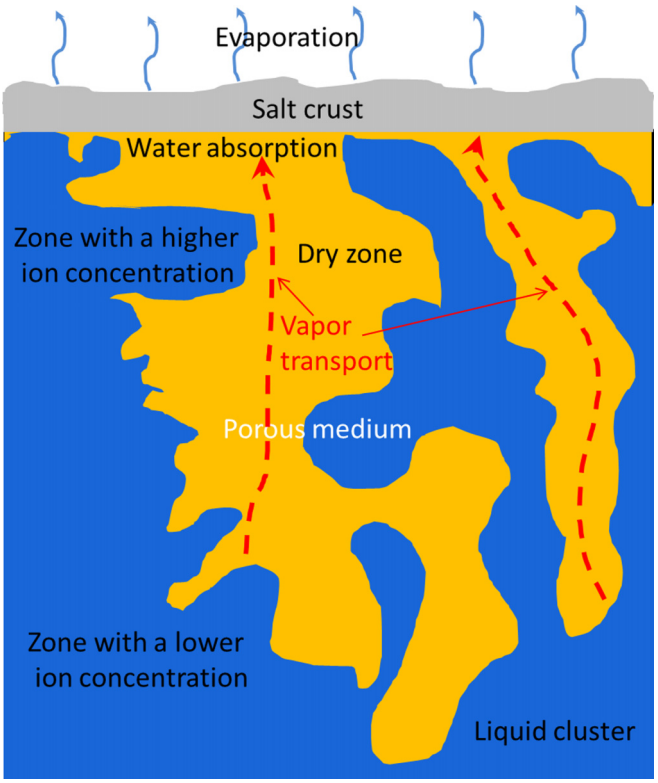

FIG. 8. Tentative sketch of a drying porous medium leading to a situation similar to that of the suspended crust experiment. The decrease in the ion mass fraction along the height of the porous medium induced a water vapor diffusive transport in the direction of the crust located on top of the porous medium where the dissolution-precipitation mechanism can take place, possibly leading to the crust upward migration and detachment.

VI. CONCLUSIONS

In summary, we have shown that dissolution-precipitation processes combined with transport phenomena can entirely explain the migration of salt crusts. This is made clear by the presented model which does not rely on any porome-chanical property of the crust. Our model proposes closed form equations enabling one to compute quantitatively the crust displacement or the growth of a porous crust surface resulting from evaporation, internal transport, and precipi-tation. It was shown in previous works, e.g., [28], that the growth of a porous salt structure was proportional to the evaporation flux. This is fully consistent with Eq. (13) which furthermore makes clear the dependence with other factors, such as the ones related to the transport of ions within the salt structure and the precipitation kinetics. It can be argued that we have presented only one experiment, thus without varying the parameters, i.e., the mean evaporation rate for instance, and use the Damköhler number Da as an adjustable parameter. Nevertheless, the value of Da leading to good agreement between the model and the experiment is quite consistent with the properties expected for the crust in the current state of the art. In this respect, more work on crust characteristics is desirable since little is actually known on the crust microstructure. Also, the suspended crust experiment is relatively delicate. This explains why we have not tried to explore a large range of parameters. We hope that the present work will stimulate further works in this direction.

Finally, it can also be noted that patterned salt crusts can form, the most famous being the Salar de Uyuni with its polygonal patterns. Explaining this pattern formation is an open problem [29]. The dissolution-precipitation mechanisms described in the present paper might also play a role in the formation of this particular pattern as well as in other crust patterns observed in nature such as blisters and domes [29].

ACKNOWLEDGMENT

The help of J. Lefort in the development of the experiment is gratefully acknowledged.

APPENDIX A: PREPROCESSING OF EXPERIMENTAL DATA

To run the model predicting the crust motion presented in Sec. IV, we only need the initial position of the crust in the cell $h_t(0)$, the initial crust thickness $h(0)$, the level of the liquid at the cell bottom $z_l(0)$, and the relative humidity $H_{r,\mathrm{inf}}(t)$ at the cell top. However, the direct use of the data measured in our experiment does not lead to very good results. For this reason, we have checked the consistency of the experimental data. As discussed in this Appendix, this led us to take into account a parasitic mass loss and to introduce a correction on $H_{r,\mathrm{inf}}(t)$. The experimental data available either from direct measurements or image processing are the following:

Mass of the system as a function of time $m(t)$ measured with a balance,

Distance between top cell and crust upper surface $h_t(t)$,

Distance between top cell and crust lower surface $h_t(t)+h(t)$,

Thickness of the crust $h(t)$,

Distance between crust lower surface and free liquid level in the cell $h_b(t)$,

Relative humidity $H_{r,\mathrm{inf}}(t)$ in the ambient air next to the cell top,

Temperature T in the ambient air ($T \sim 21\,^{\circ}\mathrm{C}$).

First we establish that the variation of the mass $m(t)$ measured by the balance corresponds to the variation of the free liquid level [the corresponding mass computed from the variation of the liquid level is denoted by $m_l(t)$]. Both masses are compared in Fig. 9. As can be seen both curves are very close which is an indication that the amount of water in the crust does not increase, or perhaps very little, during its displacement.

We have also plotted in Fig. 9(a), the variation of mass m_b corresponding to the mass transferred between the liquid level and the crust lower surface computed assuming quasisteady vapor diffusion between the two surfaces, i.e., using Eq. (1) of the main text,

$$m_b(t) = m(0) - AD_v\frac{M_v}{RT}p_{vs0}(T)\big(1-H_{r,s}\big)\int_0^t \frac{dt}{h_b(t)}, \quad \text{(A1)}$$

where $H_{r,s}=0.75$, which corresponds to a NaCl saturated solution.

As can be seen, $m_b(t) > m_l(t)$, which means that the mass loss due to evaporation from the liquid surface in the cell is less than the mass loss measured by the balance. A first option is that $H_{r,s}$ in Eq. (A1) is less than 0.75. However, this seems quite unlikely since the crust is made of crystallized salt. Another option is to assume some liquid leak (at the bottom of the cell where tightness can be imperfect). Thus we define this parasitic mass loss δm as

$$\delta m(t) = m(t) - m_b(t). \quad \text{(A2)}$$

As can be seen from Fig. 9(b), δm varies linearly, indicating a constant leak rate J_{par}. From a linear fit [red curve in Fig. 9(b)], one obtains $J_{\mathrm{par}} \approx 0.009\,22\ \mathrm{g/day}$.

Then, if there is no liquid water mass variation in the crust, the mass loss measured by the balance should also correspond to the sum of the loss by evaporation from the crust upper surface and the parasitic loss,

$$m(t) = m_t(t) + |\delta m(t)|, \quad \text{(A3)}$$

where

$$m_t = m(0) - AD_v\frac{M_v}{RT}p_{vs0}(T)\int_0^t \frac{H_{r,s}-H_{r,\mathrm{inf}}(t)}{h_t(t)}dt. \quad \text{(A4)}$$

As can be seen from Fig. 10, $m(t) < m_t(t)$ as expected, meaning that the mass loss due to evaporation from the crust top surface is less than the mass loss measured with the balance. It can also be seen that adding the parasitic loss leads to more consistent results. Finally, assuming a systematic

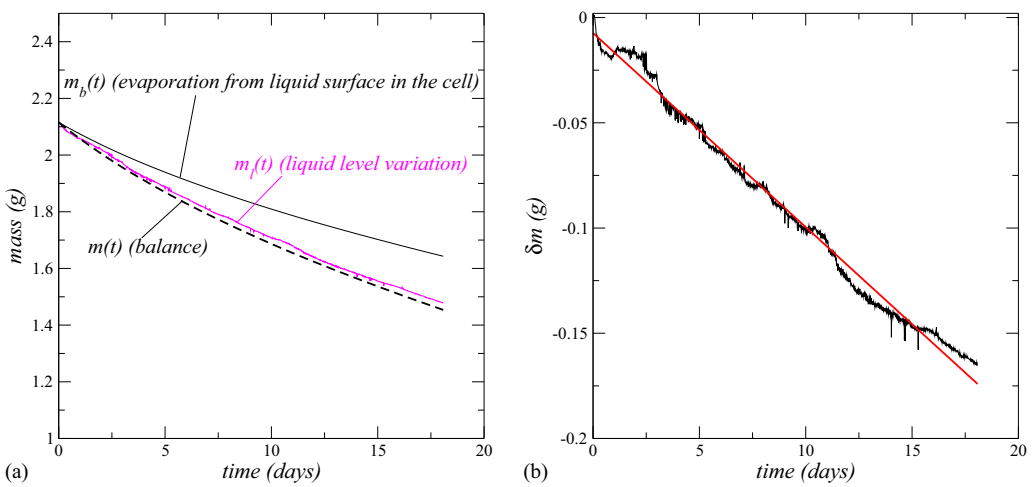

FIG. 9. (a) Mass variation as a function of time; (b) parasitic mass loss as a function of time.

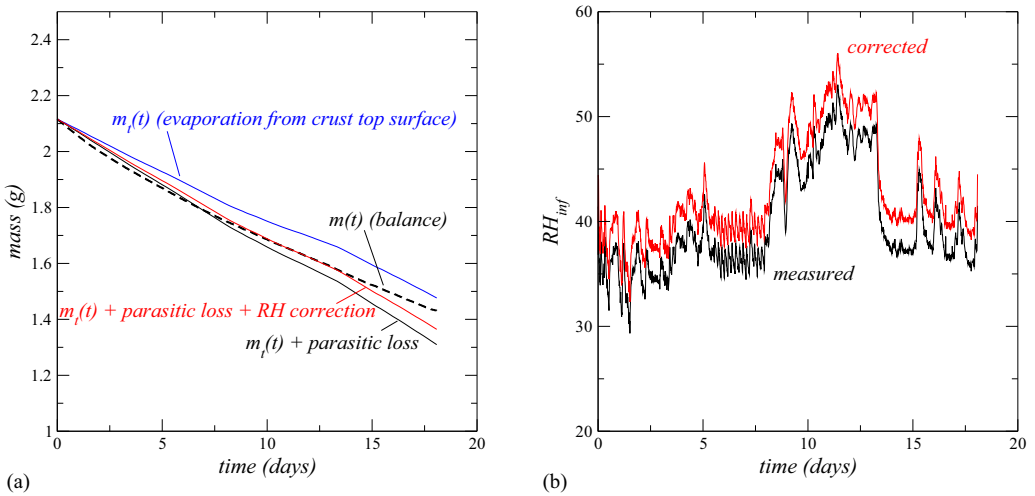

FIG. 10. (a) Mass variation as a function of time; (b) measured relative humidity variations with and without correction.

measurement error on the relative humidity $H_{r,\mathrm{inf}}(t)$ [shown in Fig. 10(b)] with $H_{r,\mathrm{infc}}(t) = H_{r,\mathrm{inf}}(t) + 0.03$ leads to the most consistent results between the available experimental data.

APPENDIX B: CLOSED-FORM EQUATIONS FOR THE CRUST TOP AND BOTTOM SURFACES VELOCITY

The ion transport within the crust is governed by the following equation:

$$\varepsilon\rho\frac{\partial C}{\partial t} + \rho V\frac{\partial C}{\partial z} = \frac{\partial}{\partial z}\left(\rho\varepsilon D_s^*\frac{\partial SC}{\partial z}\right) - (1-C)a_v\rho k_r(C - C_{\mathrm{sat}}). \tag{B1}$$

Under the assumptions of quasisteady transport and low Péclet number (see main text), Eq. (B1) is simplified as

$$\frac{\partial}{\partial z}\left(\rho\varepsilon D_s^*\frac{\partial C}{\partial z}\right) - (1-C)a_v\rho k_r(C - C_{\mathrm{sat}}) = 0. \tag{B2}$$

Neglecting the variation of density ($C \sim C_{\mathrm{sat}}$) and porosity Eq. (B2) is expressed as

$$\frac{\partial^2 C}{\partial z^2} - \frac{1}{\lambda^2}(C - C_{\mathrm{sat}}) = 0, \tag{B3}$$

where

$$\lambda^2 = \frac{\varepsilon D_s^*}{(1-C_{\mathrm{sat}})a_v k_r}. \tag{B4}$$

The boundary conditions are expressed as

$$C = C_{\mathrm{top}} \text{ at } z = z_t, \tag{B5}$$

$$C = C_{\mathrm{bot}} \text{ at } z = z_b. \tag{B6}$$

The solution of Eqs. (B3), (B5), and (B6) then reads

$$C = C_{\mathrm{sat}} + (C_{\mathrm{top}} - C_{\mathrm{sat}})\frac{\exp\left(\frac{z}{\lambda}\right) - \exp\left(-\frac{z}{\lambda}\right)}{\exp\left(\frac{h}{\lambda}\right) - \exp\left(-\frac{h}{\lambda}\right)} + (C_{\mathrm{bot}} - C_{\mathrm{sat}})\frac{\exp\left(\frac{h-z}{\lambda}\right) - \exp\left(-\frac{h-z}{\lambda}\right)}{\exp\left(\frac{h}{\lambda}\right) - \exp\left(-\frac{h}{\lambda}\right)}, \tag{B7}$$

$$\frac{\partial C}{\partial z} = \frac{(C_{\mathrm{top}} - C_{\mathrm{sat}})}{\lambda}\frac{\exp\left(\frac{z}{\lambda}\right) + \exp\left(-\frac{z}{\lambda}\right)}{\exp\left(\frac{h}{\lambda}\right) - \exp\left(-\frac{h}{\lambda}\right)} - \frac{(C_{\mathrm{bot}} - C_{\mathrm{sat}})}{\lambda}\frac{\exp\left(\frac{h-z}{\lambda}\right) + \exp\left(-\frac{h-z}{\lambda}\right)}{\exp\left(\frac{h}{\lambda}\right) - \exp\left(-\frac{h}{\lambda}\right)}. \tag{B8}$$

Then noting that $\exp(\frac{h}{\lambda}) \gg \exp(-\frac{h}{\lambda})$ when $\lambda < h$, the above equations are expressed as

$$C = C_{\mathrm{sat}} + (C_{\mathrm{top}} - C_{\mathrm{sat}})\left[\exp\left(-\frac{h-z}{\lambda}\right) - \exp\left(-\frac{h+z}{\lambda}\right)\right] + (C_{\mathrm{bot}} - C_{\mathrm{sat}})\left[\exp\left(-\frac{z}{\lambda}\right) - \exp\left(-\frac{2h-z}{\lambda}\right)\right], \tag{B9}$$

$$\rho\varepsilon D_s^*\frac{\partial C}{\partial z}\bigg|_{z=h} \approx \rho\varepsilon D_s^*\frac{(C_{\mathrm{top}} - C_{\mathrm{sat}})}{\lambda}, \tag{B10}$$

$$\rho\varepsilon D_s^*\frac{\partial C}{\partial z}\bigg|_{z=0} \approx \rho\varepsilon D_s^*\frac{(C_{\mathrm{sat}} - C_{\mathrm{bot}})}{\lambda}. \tag{B11}$$

In this limit, Eqs. (8) and (9) in the main text can be expressed as

$$\frac{dz_t}{dt} \approx \frac{C_{\mathrm{sat}} j_t - \rho\varepsilon D_s^*\frac{(C_{\mathrm{top}} - C_{\mathrm{sat}})}{\lambda}}{\rho_{\mathrm{cr}}(1-\varepsilon)(1-C_{\mathrm{sat}})} \approx \frac{\rho}{\rho_{\mathrm{cr}}}k_r(C_{\mathrm{top}} - C_{\mathrm{sat}}), \tag{B12}$$

$$\frac{dz_b}{dt} \approx \frac{C_{\mathrm{sat}} j_b - \rho\varepsilon S D_s^*\frac{(C_{\mathrm{sat}} - C_{\mathrm{bot}})}{\lambda}}{\rho_{\mathrm{cr}}(1-\varepsilon)(1-C_{\mathrm{sat}})} \approx \frac{\rho}{\rho_{\mathrm{cr}}}k_r(C_{\mathrm{sat}} - C_{\mathrm{bot}}), \tag{B13}$$

which give an estimate of the ion mass fraction at the bottom and the top,

$$(C_{\mathrm{top}} - C_{\mathrm{sat}}) \approx \frac{C_{\mathrm{sat}} j_t}{\rho(1-\varepsilon)(1-C_{\mathrm{sat}})k_r + \frac{\rho\varepsilon D_s^*}{\lambda}}. \tag{B14}$$

$$(C_{\mathrm{sat}} - C_{\mathrm{bot}}) \approx \frac{C_{\mathrm{sat}} j_b}{\rho(1-\varepsilon)(1-C_{\mathrm{sat}})k_r + \frac{\rho\varepsilon D_s^*}{\lambda}}. \tag{B15}$$

Using Eqs. (B14) and (B15) and taking into account Eq. (B4) leads to expressing Eqs. (B12) and (B13) as

$$\frac{dz_t}{dt} \approx \frac{C_{\rm sat} j_t}{\rho_{\rm cr}(1-\varepsilon)(1-C_{\rm sat})}\left[\frac{(1-\varepsilon)(1-C_{\rm sat})\lambda k_r}{(1-\varepsilon)(1-C_{\rm sat})\lambda k_r + \varepsilon D_s^*}\right], \tag{B16}$$

$$\frac{dz_b}{dt} \approx \frac{C_{\rm sat} j_b}{\rho_{\rm cr}(1-\varepsilon)(1-C_{\rm sat})}\left[\frac{(1-\varepsilon)(1-C_{\rm sat})\lambda k_r}{(1-\varepsilon)(1-C_{\rm sat})\lambda k_r + \varepsilon D_s^*}\right], \tag{B17}$$

which after introduction of the Damköhler number $\mathrm{Da} = \frac{(1-\varepsilon)(1-C_{\rm sat})\lambda k_r}{\varepsilon D_s^*}$ leads to Eqs. (13) and (14) in the main text.

[1] X. Y. Chen, Aust. J. Soil Res. **30**, 429 (1992).
[2] U. Nachshon, N. Weisbrod, M. I. Dragila, and A. Grader, Water Resour. Res. **47**, W03513 (2011).
[3] A. S. Goudies and H. A. Viles, *Salt Weathering Hazards* (Wiley, Chichester, UK, 1997).
[4] R. J. Flatt, F. Caruso, A. M. A. Sanchez, and G. W. Scherer, Nat. Commun. **5**, 4823 (2014).
[5] M. Schiro, E. Ruiz-Agudo, and C. Rodriguez-Navarro, Phys. Rev. Lett. **109**, 265503 (2012).
[6] G. W. Scherer, Cem. Concr. Res. **34**, 1613 (2004).
[7] E. E. Alonso and A. Ramon, Geotechnique **63**, 857 (2013).
[8] H. Eloukabi, N. Sghaier, S. Ben Nasrallah, and M. Prat, Int. J. Heat Mass Transfer **56**, 80 (2013).
[9] S. Gupta, H. Huinink, M. Prat, L. Pel, and K. Kopinga, Chem. Eng. Sci. **109**, 204 (2014).
[10] H. Fujimaki, T. Shimano, M. Inoue, and K. Nakane, Vadose Zone J. **5**, 1246 (2006).
[11] S. Veran-Tissoires and M. Prat, J. Fluid Mech. **749**, 701 (2014).
[12] S. Shokri-Kuehni, T. Vetter, C. Webb, and N. Shokri, Geophys. Res. Lett. **44**, 5504 (2017).
[13] J. Desarnaud, H. Derluyn, L. Molari, S. de Miranda, V. Cnudde, and N. Shahidzadeh, J. Appl. Phys. **118**, 114901 (2015).
[14] T. Corti and U. K. Krieger, Appl. Opt. **46**, 5835 (2007).
[15] U. Nachshon, N. Weisbrod, R. Katzir, and A. Nasser, Geophys. Res. Lett. **45**, 6100 (2018).
[16] S. Dai, H. Shin, and J. C. Santamarina, Acta Geotech. **11**, 1103 (2016).
[17] A. Naillon, P. Joseph, and M. Prat, Phys. Rev. Lett. **120**, 034502 (2018).
[18] W. J. P. Van Enckevort and J. H. Los, Cryst. Growth Des. **13**, 1838 (2013).
[19] See Supplemental Material at http://link.aps.org/supplemental/10.1103/PhysRevE.100.032802 for a movie showing the crust migration.
[20] J. Bear, *Dynamics of Fluids in Porous Media* (Dover Publications, New York, 1972).
[21] J. C. Slattery, *Momentum, Energy and Mass Transfer in Continua* (McGraw-Hill, New York, 1972).
[22] F. J. Valdés-Parada, B. Goyeau, and J. A. Ochoa-Tapia, Chem. Eng. Sci. **61**, 1692 (2006).
[23] J. W. Mullin, *Crystallization*, 4th ed. (Butterworth Heinemann, Oxford, UK, 2001).
[24] H. P. Huinink, L. Pel, and M. A. J. Michels, Phys. Fluids **14**, 1389 (2002).
[25] A. Naillon, P. Joseph, and M. Prat, J. Cryst. Growth **463**, 201 (2017).
[26] F. A. L. Dullien, *Porous Media: Fluid Transport and Pore Structure*, 2nd ed. (Academic Press, San Diego, CA, 1992).
[27] J.-H. Kim, J. A. Ochoa, and S. Whitaker, Transp. Porous Media **2**, 327 (1987).
[28] N. Sghaier, S. Geoffroy, M. Prat, H. Eloukabi, and S. Ben Nasrallah, Phys. Rev. E **90**, 042402 (2014).
[29] T. M. Goodall, C. P. North, and K. W. Glennie, Sedimentology **47**, 99 (2000).